DARPA/ONR Grant #N00014-91-J-1976

Second Quarterly Progress Report
(covering the period of November 1, 91 - January 31, 1992)

Project Title: Development of Ultra-Low Noise, High Sensitivity Planar Metal Grating Coupled AlGaAs/GaAs Multiquantum Well IR Detectors for Focal Plane Array Staring IR Sensor Systems

Submitted to

Max N. Yoder
Office of Naval Research
Code 1114 SS
800 North Quincy Street
Arlington, VA 22217-5000

Prepared by

Prof. Sheng S. Li

Dept. of Electrical Engineering
University of Florida
Gainesville, Florida 32611

Tel.(904)-392-4937
Fax(904)-392-8671

February 1, 1992

I. Introduction

During this reporting period (11-01-91 to 1-31-92), we have continued the study of the performance characteristics of the metal grating coupled bound-to-miniband (BTM) and step-bound-to-miniband (SBTM) transition multiquantum well(MQW)/superlattice (SL) barrier infrared (IR) detectors formed on the GaAs and InP substrates for 8 - 12 μm focal plane arrays and image sensor applications. Specific tasks performed included: (1) designed and grown several (BTM) GaAs- and (SBTM) InGaAs-based QWIP (quantum-well infrared photodetector) structures by MBE technique, (2) fabricated the metal grating couplers on the QWIP's described in (1) with different granting periodicities (1.1, 3.2, 5, 7.2, and 10 μm) and patterns (line and cross gratings), (3) performed theoretical and experimental study of the light coupling quantum efficiency vs. grating periodicities for the QWIP's, and (4) performed theoretical and experimental study of the dark current vs. temperature for the GaAs QWIP's. Detailed results are discussed in Section III.

We have grown two types of BTM and SBTM transition InGaAs QWIPs by using the molecular beam epitaxy (MBE) technique. The SBTM QWIP uses a lightly strained $In_{0.07}Ga_{0.93}As$ quantum well with a short-period superlattice $Al_{0.4}Ga_{0.6}As/GaAs$ barrier grown on GaAs substrate, and the BTM QWIP uses an InP lattice-matched enlarged $In_{0.47}Ga_{0.53}As$ quantum well with a short-period superlattice $In_{0.48}Ga_{0.52}As/In_{0.47}Ga_{0.53}As$ barrier grown on InP substrate. The results for the SBTM QWIPs showed that dark current at 77 K was 10 times lower than the conventional QWIP reported in the literature, and the BTM QWIP showed a largely enhanced intersubband absorption at 10.73 μm (demonstrated for the first time in InGaAs). The detectivity for the SBTM QWIP structure measured at Brewster angle was found to be 2.1×10^{10} $cm\sqrt{Hz}/W$ at $V_b = 5$ V and T = 63 K. To investigate the performance characteristics of the InGaAs BTM QWIPs, we have grown three InP-based BTM QWIP's structures with three dopant concentrations used in the InGaAs quantum wells (i.e., undoped, 5×10^{17}, and 2×10^{18} cm^{-3}). Device fabrication on these wafers is currently being undertaken, and measurements of the performance characteristics will be carried out in the nexte reporting period. To develop the planar metal grating couplers for the top and back illumination on the QWIPs, we have designed and fabricated 8 new photomasks with different grating patterns and periodicities. These new masks are currently

being used in the proposed study of light coupling efficiency versus grating periodicity in the large area QWIPs.

II. Achievements and Publications

Specific accomplishments and publications are summarized as follows:

2.1 Research Accomplishments:

- Performed a theoretical and experimental study of the light coupling quantum efficiency versus grating periodicities for the planar metal grating coupled GaAs/AlGaAs QWIPs under normal incident illumination. A peak coupling quantum efficiency of 11 % was obtained for the 5 μm grating periodicity. Five different grating periodicities with Λ = 1.1, 3.2, 5, 7, and 10 μm were used in the present study, and the results are discussed in Section 3.1.

- Performed theoretical and experimental studies of the dark current versus temperature and bias voltage in the BTM and SBTM QWIPs. The results reveal that thermionic emission is dominant current conduction mechanism at higher temperatures (e.g., $T \geq$ 60 K) and the resonant tunneling current prevails at low temperatures (e.g., $T \leq$ 40 K). Excellent agreement between our theoretical calculations and experimental data was obtained for both detector structures. A paper on this study has been submitted to Journal of Applied Physics for publication. Details of this study are discussed in Section 3.2.

- Performed cross sectional Transmission Electron Microscopy (TEM) analysis on several BTM and SBTM QWIP structures. A typical cross sectional transmission electron microscopy (TEM) photograph for an InGaAs quantum well/InAlAs-InGaAs superlattice barrier QWIP is shown in Fig. 2.1.

- Performed the dark current, absorption, and photoresponse measurements on the SBTM QWIPs. A reduction of the detector's dark current by a factor of 10 over the conventional QWIP has been achieved in this detector. The detectivity for this SBTM QWIP measured at Brewster angle was found to be 2.1×10^{10} cm$\sqrt{Hz}$/W at

$V_b = 5$ V and T = 63 K. A paper on this QWIP's will be published in the February issue of Appl. Phys. Lett. (1992).

- Designed and grown an InP lattice-matched InGaAs quantum well with short-period superlattice InAlAs/InGaAs barrier QWIP structure with three different doping concentrations in the quantum wells. The intersubband optical absorption property in this QWIP has been studied. A strong intersubband infrared absorption at room temperature and $\lambda = 10.73$ μm has been observed for the first time in this structure. An integrated optical absorption strength of $I_A = 19.5$ Abs-cm$_{-1}$ was obtained at the Brewster's angle $\theta_B = 74.5^o$, which is about five times larger than that of the conventional single bound-to-bound transition. The results clearly indicate that the enlarged quantum well and the broad miniband are superior for large infrared absorption and detection. A paper on the intersubband absorption in this detector structure has been published in Appl. Phys. Lett, Nov. issue, 1991. To evaluate the performance characteristics of this new detector structure, we have grown three QWIPs using this structure with different doping concentrations in the InGaAs quantum well (i.e., undoped, 5×10^{17}, and 2.2×10^{18} cm^{-3}). Device fabrication and characterization on these three QWIP samples will be made in the next reporting period, and the results will be discussed in the next quarterly report.

2.2. Journal and Conference Papers:

1. Larry S. Yu and Sheng S. Li,"A Low Dark Current, High Detectivity, Grating Coupled AlGaAs/GaAs Mulitple Quantum Well IR Detector Using Bound-to-Miniband Transition for 10 μm Detection,"Appl. Phys. Lett., 59 (11),p.1332, Sept.9 1991.

2. Larry. S. Yu. Sheng S. Li, and Pin Ho "Largely Enhanced Bound-to-Miniband Absorption in an InGaAs Multiple Quantum Well with Short-Period Superlattice InAlAs/InGaAs Barrier " Applied Physics Lett., 59(21), p.2712, Nov. 18, 1991.

3. Larry S. Yu, Y. H. Wang, Sheng S. Li and Pin Ho,"A Low Dark Current Step-Bound-to-Miniband Transition InGaAs/GaAs/AlGaAs Multiquantum Well Infrared Detector," Appl. Phys. Lett., 60(8), 24 Feb., 1992.

4. Larry S. Yu, Sheng S. Li, Y. H. Wang, and Y. C. Kao,"A Study of the Coupling Efficiency versus Grating Periodicity in A Normal Incident GaAs/AlGaAs Multiquantum Well Infrared Detector," submitted. J. Appl. Phys., Jan. 9, 1992.

5. Larry S. Yu, Sheng S. Li, and Pin Ho, " Obervation of Large Intra-subband Absorption in an InGaAs Multiple Quantum Well with Short-Period Superlattice InAlAs/InGaAs Barrier," paper to be presented at the *SPIE'S 1992 SYMPOSIUM on Quantum Wells and Superlattices*, Somerset, NJ, 23-27 March,1992. Paper to be appeared in conf. proceeding.

6. Sheng S. Li and Larry S. Yu,"A New Class of Bound-to-Miniband Transition III-V Multiquantum Well Infrared Detectors," paper to be presented at *the Conference on Infrared Detectors and Focal Plane Arrays at OE/Aerospace Sensing 92*," Orlando, FL, April 20-24, 1992. Paper to be published in the conference proceeding.

2.3. Workshop and Conference

1. Dr. Li plans to attend the ***Innovative Long-Wavelength Infrared Detector Workshop***, to be held in (JPL) Pasadena CA, April 7-9, 1992.

2. Dr. Li plans to attend and and present a QWIP paper at *the International Conference on Narrow Gap Semiconductors* to be held at University of South Hampton. UK, July 19-23, 1992.

3. Dr. Li has been asked to give an invited paper at *the International IR Detector Workshop*, to be held in Vancouver, Canada, September 7-10, 1993.

2.4 Interactions with Industrial Research Laboratories

1. Continued collaborating with Dr. Pin Ho of General Electric Co., in Syracuse NY to grow the III-V multiquantum IR detector structures for us by molecular beam epitaxy (MBE) technique. The results so far have produced several journal and conference papers. Several new QWIP's have been grown recently, and will be processed into devices in the next reporting period for evaluation.

2. Continued collaborating with Dr. Y. C. Kao on the growth of quantum-well IR detector structures by MBE technique. We plan to continue this collaboration, and new design will be sent to Dr. Kao to grow the new QWIP structures for us.

3. Continued collaborating and exchanging technical information and IR detector papers with Dr. Barry Levine of A T & T Bell Laboratories. We have recently sent several of our QWIPs samples to Dr. Levine for evaluation of the performance characteristics of our QWIPs. We expect this collaboration and exchange of information to strengthen in the months ahead.

III. Technical Results and Discussion

3.1 A Study of the Coupling Efficiency versus Grating Periodicity In A Normal Incident GaAs/AlGaAs QWIP's

A detailed study of the dependence of coupling quantum efficiency on the grating periodicity of a planar metal grating coupled BTM transition GaAs/AlGaAs QWIP's has been made in this work. Five samples with different grating periodicities of Λ = 1.1 , 3.2, 5, 7, and 10 μm have been used in this study. The results showed that the device with a 5 μm grating periodicity yielded the best front side coupling efficiency, which is in good agreement with our theoretical prediction. A single pass quantum efficiency (η) as high as 11 % was obtained for the front side illumination at λ_p = 9.8 μm and T = 77 K.

There has been a considerable interest in the edge illuminated long wavelength quantum well infrared photodetectors (QWIPs) and modulators in the atmospheric window of 8 - 12 μm[1-14]. Several studies on the phase modulated reflection metal grating coupled QWIPs and arrays using a back side illumination have been reported. [15-17] Recently, we have demonstrated an amplitude modulated metal grating coupled AlGaAs/GaAs QWIP with a front normal illumination[18-20]. A thin (0.1 μm) metal grating contact structure is formed on the detector surface to serve both as an effective infrared light coupler and as ohmic contacts. The main advantage of using a metal grating structure is that the vector of electric field on the metal grating is always perpendicular to the metal surface which is essential for enhancing the intersubband absorption in the quantum well detectors. Using a 5 μm grating periodicity,

a peak detectivity $D^* = 1.6 \times 10^{10}$ cm$\sqrt{Hz}$/W has been obtained at $\lambda_p = 8.9$ μm and T = 77 K with front side normal illumination. This simple but extremely uniformed planar metal grating coupled structure is indeed highly desirable for use in the large area infrared detector arrays and image sensors.

It is well known that electric dipole matrix element existing between the subbands of a quantum well is relatively large. However, since only the component of IR radiation with electric field $\vec{\mathcal{E}}_\perp$ vector perpendicular to the quantum well layers will give rise to intersubband transition in the quantum wells, no intersubband infrared absorption in the quantum wells is expected in the ordinarily bare surface at normal incidence. Even tilted 73° at the Brewster's angle, due to the large refractive index (n = 3.3) of GaAs and the anisotropic character of the absorption, only a small fraction, $\cos^2(\theta_B)/\sin(\theta_B) = 9\%$, of the total transverse magnetic (TM) field intensity can be absorbed. In fact, the practical net absorption is only about 4%. For a large and uniformed surface illumination, a textured diffraction surface, or metal grating, is needed to induce the perpendicular electric field component for intersubband resonance[21].

The key parameter which controls the coupling quantum efficiency of a planar metal grating structure under normal incident IR illumination is the grating periodicity. In general, the coupling quantum efficiency is a strong function of the grating periodicity for a given wavelength. The amplitudes of the transmitted waves and the diffracted angles could vary significantly with a change of the grating periodicity. Therefore, the performance of a QWIP can be greatly influenced by varying the grating periodicity for the top contacts in the detector. The purpose of this paper is to conduct a theoretical and experimental study of the relationship between the coupling quantum efficiency and the grating periodicity in a normal incident GaAs/AlGaAs quantum well IR detector at 8 – 10 μm wavelength range. The results of this study should be useful for designing the normal incident metal grating coupled QWIPs for long wavelength infrared focal plane arrays and sensing applications.

The GaAs/AlGaAs QWIP structure was grown by using the molecular beam epitaxy (MBE) technique. The growth sequence for the GaAs/AlGaAs QWIP's structure started with a 1.0 μm buffer layer of n-GaAs (1.4×10^{18} cm^{-3}) grown on a semi-insulating (S.I.) GaAs substrate. This was followed by the growth of a 40-period of multiquantum wells

with alternating doped ($n = 1.4 \times 10^{18}\ cm^{-3}$) GaAs quantum well layer width of 39 Å and undoped $Al_{0.25}Ga_{0.75}As$ barrier layer width of 490 Å. Finally, an n^+-GaAs cap layer of 0.1 μm thick and dopant density of $2.0 \times 10^{18}\ cm^{-3}$ was grown on top of the multiquantum well layer structure. To facilitate the photocurrent measurements, the mesa-etched detector arrays were made on the highly doped GaAs buffer layer. The area of each detector is 200 $\times$ 200 μm^2. The ohmic contacts were formed by evaporating Au-Ge/Ni/Au films on the heavily-doped GaAs layers. A set of metal grating contacts with different periodicities of 1.1, 3.2, 5, 7, and 10 μm were deposited onto the n^+-type GaAs cap layer by using electron beam evaporation to form the top ohmic contacts.

As shown in Fig. 3.1, it is assumed that the metal strips in the grating contact structure have a large electrical conductivity σ and a negligible thickness ($h \rightarrow 0$). The metal is equivalent to a lossy dielectric with relative permittivity $\epsilon = 1 + i\sigma/\epsilon_o\omega$. When a normal incident infrared light is impinging upon the grating surface, the corresponding transmission magnetic field in the GaAs/AlGaAs quantum well region can be expressed by[22]

$$H_t(y,z) = T_0 e^{ikz} + \sum_{m=1}^{\infty} T_m cos(8m\pi y/\Lambda) e^{i\Gamma_m z} \tag{1}$$

where T_0 is the zeroth order transmission coefficient, Γ_m is the Gamma function of order m, and T_m ($m = 1, 2, \cdots$) is the high order transmitted wave amplitudes which can be written as

$$T_{2n} = (-1)^n \frac{K_+(k)K_+(\Gamma_{2n})}{2\Gamma_{2n}(k+\Gamma_{2n})} t, \qquad n = 1, 2, \cdots \tag{2}$$

$$T_{2n-1} = (-1)^n \frac{K_+(k)(k+\Gamma_{2n-1})}{(2n-1)\pi\Gamma_{2n-1}K_+(\Gamma_{2n-1})} t, \qquad n = 1, 2, \cdots \tag{3}$$

where t is the transmission coefficient at the GaAs surface and K_+ is given by

$$K_+^{-1} = (w+k)^{-1} \prod_{n=1}^{\infty} \frac{w+\Gamma_{2n-1}}{w+\Gamma_{2n}} \frac{2n}{2n-1} \tag{4}$$

The grating coupling equation for the forward-diffracted (transmitted) waves can be written as[23]

$$n_1 sin\theta_t^{(m)} = n_0 sin\theta_i - \frac{m\lambda}{\Lambda} sin\phi \tag{5}$$

where n_0 and n_1 denote the optical refractive indices of layers above and beneath the grating layer, respectively, and are given by $n_0 = \sqrt{\epsilon_0}$ and $n_1 = \sqrt{\epsilon_1}$. The cutoff periodicity Λ_c for

the mth diffracted mode for a given incident angle θ can be estimated by using the relation

$$\Lambda_c = \left| \frac{\pm m\lambda}{\pm sin\theta_i - (\epsilon_1)^{1/2}} \right| \qquad m = 0, 1, 2, \cdots \tag{6}$$

where λ is the incident wavelength, ϵ_1 is the dielectric constant of GaAs which is equal to 10.7. Substituting [??] into Eq.(6), the first three cutoff periodicities for the incident wavelength of 9.8 μm under normal incidence were found to be roughly equal to 3, 6, and 9 μm, respectively.

The angle dependence of the intersubband optical absorption coefficient α as a function of the mth diffracted angle θ_t^m in the multiple quantum well layers can be found by using the relation[24]

$$\alpha[\theta_t^{(m)}] = \frac{e\omega\mu cm^* I}{n_3 L'_{EW}\pi\hbar^2} \cos^2\theta_t^{(m)} \tag{7}$$

where m^* is the electron effective mass for GaAs; μ is the permeability; L'_{EW} is the effective width of the infinity potential quantum well which is slightly larger than the finite potential well width; c is the speed of light in free space; I is the relative transition probability between the ground state and the miniband state which is given by

$$I = \int_0^\infty dE \frac{\langle z\rangle^2 (f_1 - f_2)\Gamma_{12}}{(E_2 - E_1 - E_{xch} - \hbar\omega)^2 + (\Gamma_{12})^2} \tag{8}$$

where $2\Gamma_{12}$ is the intersubband full width at half maximum (FWHM); $\langle z\rangle$ is the dipole matrix element; E_{xch} is the exchange energy due to the high doping concentration; $f_{1,2}$ is the Fermi function given as $f_{1,2} = [1 - exp(E_{1,2} - E_f)/kT]^{-1}$; E_f is the Fermi level; k is the Boltzman constant; E_1 and E_2 are the energy eigenvalues of the subbands in the quantum well, which can be found by using the transfer matrix method[18]. For our present structure, the parameters used in the calculation are: $E_1 = 96$ meV, $E_2 = 210$ meV, $E_{xch} = 10$ meV, $E_f = 102.8$ meV, $n_3 = 3.3$, $m^* = 0.0665$ m_0, $L'_{EW} = 62$ Å, $2\Gamma_{12} = 20$ meV, and T = 77 K. Fig.3.2 shows the calculated angle dependence of the intersubband absorption coefficient $\alpha(\lambda, \theta_t)$ under diffracted angles $\theta_t = 90°$, 50°, and 25°, respectively. The photocurrent responsivity R_λ of the multiquantum well IR detectors can be expressed as

$$R_\lambda(\Lambda) = \eta(\Lambda) \cdot \frac{e\lambda}{hc} G, \qquad (A/W) \tag{9}$$

where e is the electronic charge; G is the photoconductive gain; η is the detector's quantum

efficiency which can be determined by using the expression

$$\eta(\Lambda) = \frac{1}{2}\sum_m \frac{\Gamma_m |T_m(\Lambda)|^2}{2k}\{1 - e^{-\alpha(\theta_t^{(m)}(\Lambda))L}\} \qquad (10)$$

where L is the total length of the superlattice absorption region. A factor of 1/2 in front of the summation above is included to account for the reduction of an unpolarized light source. By substituting Eqs. (2), (3), and (6) into (9), we obtain a normal incident single pass quantum efficiency of 11 %, 1.4 %, and 8.3% for the samples with grating periodicities of 5, 7, and 10 μm, respectively, at the peak wavelength $\lambda_p = 9.8$ μm and operating temperature T = 77 K. When an incident light is polarized along the direction perpendicular to the grating strips, the quantum efficiency will increase by a fact of two, which yields $\eta = 22$ % for a 5 μm grating coupled IR detector under the front side illumination. We shall next discuss the results of our measurements on these QWIPs samples.

Figure 3.3 shows one of the fabricated planar grating patterns, which has a grating periodicity equal to 5 μm. Measurements of detector performance and characteristics were made in a close-cycled liquid-helium cryogenic dewar. The photocurrent was measured as a function of temperature, wavelength, and applied bias, using a CVI Laser Digikrom 240 monochromator and an ORIEL ceramic element infrared source. Due to the very large device resistance and very small values of dark current I_d present in the device at 77 K, the short-circuit measurements were used to determine the photocurrent I_{ph}[10]. Since the metal surface only has a normal electric field vector, the x-component of the IR radiation, $\vec{\mathcal{E}}_x$, is zero in the highly conductive regime. Therefore, the IR beam is spatially modulated in the near field of the grating, and has a z- component of the electric field $\vec{\mathcal{E}}_z$ which can induce perpendicular excitation of intersubband resonance. It is noted that the optimal grating periodicity is obtained for a grating periodicity which is neither too small nor too close to the incident IR radiation wavelength. We have found that a grating periodicity of $\Lambda = 5$ μm gives the best front coupling efficiency, followed by 10, 7, 3.2, and 1.1μm. This is illustrated in Figure 3.4 for the grating enhanced intersubband excitation at normal incidence. The peak wavelength was found around 9.8 μm with its cutoff wavelength around 10.8 μm at T = 77 K. The backside illumination experiment was conducted by illuminating the infrared light through the S.I. GaAs substrate surface. The results revealed that the measured responsivities for the tested samples are quite similar to those of the front illuminated samples for most of

the grating periodicities. However, the results also showed that the 7 μm grating periodicity yielded the best coupling efficiency for the backside illumination.

We also measured the angle dependence of the photocurrent in our grating coupled GaAs/AlGaAs quantum well IR detectors. Figure 3.5 shows the relative photocurrent as a functions of the incident angle θ, for the detector using a 5 μm grating coupler. Similar measurement was also performed for the device with a 7 μm grating coupler, and the result is shown in Figure 3.6. The relatively slow variation with respect to the incident angle indicates that there are more than one higher order modes passing through the grating slit and propagating into the quantum well layers, or the first transmitted TM mode is far from the cutoff frequency. The results further suggest that the high conducting metal strip grating can be used effectively not only as a high-efficiency transmission coupler for front side normal illumination but also as an efficient reflection coupler for the backside illumination.

The advantages of using the front surface grating structure include: (1) it can eliminate the undesirable cross-talk in the detector arrays and clear the infrared image from the effect of multiple images; (2) the planar metal gratings, unlike deeply etched spatial gratings, offer extremely thin and smooth surface quality, which is good for surface passivation and antireflection coatings; (3) the planar structure is also highly desirable for large integration and high-speed applications; (4) the strip-metal grating coupler structure does not need extra epitaxial layer (whose thickness is usually much larger than the active multi-quantum well layer itself) for chemical etching. Therefore, it can significantly cut down the molecular beam epitaxy (MBE) growth time and material exhaustion. Therefore, a new type of low cost, high yield, and large area long wavelength infrared detector array can be realized by using our metal grating coupled GaAs/AlGaAs MQW detector structure.

In conclusion, we have performed a detailed theoretical and experimental study on the effect of grating periodicity on the coupling quantum efficiency in the normal incident planar metal grating coupled GaAs/AlGaAs quantum well IR detectors in the 8 - 12 μm wavelengths. The dependence of the responsivity and quantum efficiency on the grating periodicity for these IR detectors have been investigated. The results showed that the optimal grating periodicity for these MQW IR detectors is about 5 μm for the front side normal illumination and 7 μm for the backside illumination case. A single pass quantum efficiency

as high as 11 % has been achieved for the 5 μm grating coupled GaAs/AlGaAs MQW infrared detector, which is in good agreement with our theoretical prediction. The advantages of high uniformity, low cost, high yield, and elimination of cross-talk offered by using a planar metal grating coupler structure are essential for developing high quality GaAs/AlGaAs QWIP arrays and image sensors for long wavelength infrared applications.

REFERENCES

1. J. S. Smith, L.C. Chiu, S. Margalit, A. Yariv,and A. Y. Cho, J. Vac. Sci. Technol. B 1, 376 (1983).

2. B. F. Levine, K.K. Choi, C.G. Bethea, J. Walker, and R.J. Malik, Appl. Phys. Lett. **50**, 1092 (1987).

3. Larry S. Yu, Sheng S. Li,and Pin Hu, Appl. Phys. Lett. **59**, 2712 (1991).

4. Larry S. Yu, Sheng S. Li, Y.H. Wang, and Pin Hu, Appl. Phys. Lett., *to appear in the issue of* Feb. 24 (1992).

5. D.D. Coon and R. P. G. Karunasiri, Appl. Phys. Lett. 33, 495 (1984).

6. B. F. Levine, G. Hasnain, C.G. Bethea, and Naresh Chand, Appl. Phys. Lett., 54, 2704 (1989).

7. G. Hasnain, B.F. Levine, S. Gunapala, and Naresh Chand, Appl. Phys. Lett., 57, 608 (1990).

8. S.D. Gunapala, B.F. Levine, and Naresh Chand, Appl. Phys. Lett., 70, 305 (1991).

9. A. Zussman, B.F. Levine, J.M. Kuo, and J. de Jong, Appl. Phys. Lett., 70, 5101 (1991).

10. B.K. Janousek, M.J. Daugherty, W.L. Bloss, M.L. Rosenbluth, M.J. O'Loughlin, H. Kanter, F.J. De Luccia, and L.E. Perry, J. Appl. Phys. 67, 7608 (1991).

11. A. Kastalsky, T. Duffield, S. J. Allen, and J. Harbison, Appl. Phys. Lett., 52, 1320 (1988).

12. G. Hasnain, B.F. Levine, C.G. Bethea, R.R. Abbott, and S.J. Hsieh, J. Appl. Phys., 67, 4361 (1990).

13. R.P.G. Karunasiri, J.S. Park, and K.L. Wang, Appl. Phys. Lett., 59, 2588 (1991).

14. F.H. Julien, P. Vagos, J.-M. Lourtioz, and D.D.Yang, Appl. Phys. Lett., 59, 2645 (1991).

15. K.W. Gossen and S.A. Lyon, Appl. Phys. Lett., 53, 1027 (1988).

16. G. Hasnain, B.F. Levine, C.G. Bethea, R.A. Logan, J. Walker, and R.J. Malik, Appl. Phys. Lett., 54, 2515 (1989).

17. Andersson, L. Lundqvist, and Z.F. Paska, Appl. Phys. Lett., 59, 859 (1991).

18. Larry S. Yu, Sheng S. Li, Y.C. Kao, *Proc. Government Microcircuit Applications Conference* (GOMAC) (Las Vegas, NV, 1990), pp. 479.

19. Larry.S. Yu, Sheng S. Li, Appl. Phys. Lett. 59, 1332 (1991).

20. Larry S. Yu, Sheng S. Li, and Y.C. Kao, *Proc. International Electron Devices and Materials Symposium* (Hsinchu, Taiwan, 1990), pp. 472.

21. T.W. Nee and F. Koch, Phys. Rev. B 29, 3225 (1984).

22. D. Maystre and R. Petit, Opt. Commu. 5, 91 (1972).

23. R. Petit, *Electromagnetic Theory of Gratings*, (Springer-Varlag, Berlin, 1980).

24. D. Ahn and S.L. Chuang, IEEE J. Quantum Electron., QE-23, 2196 (1987).

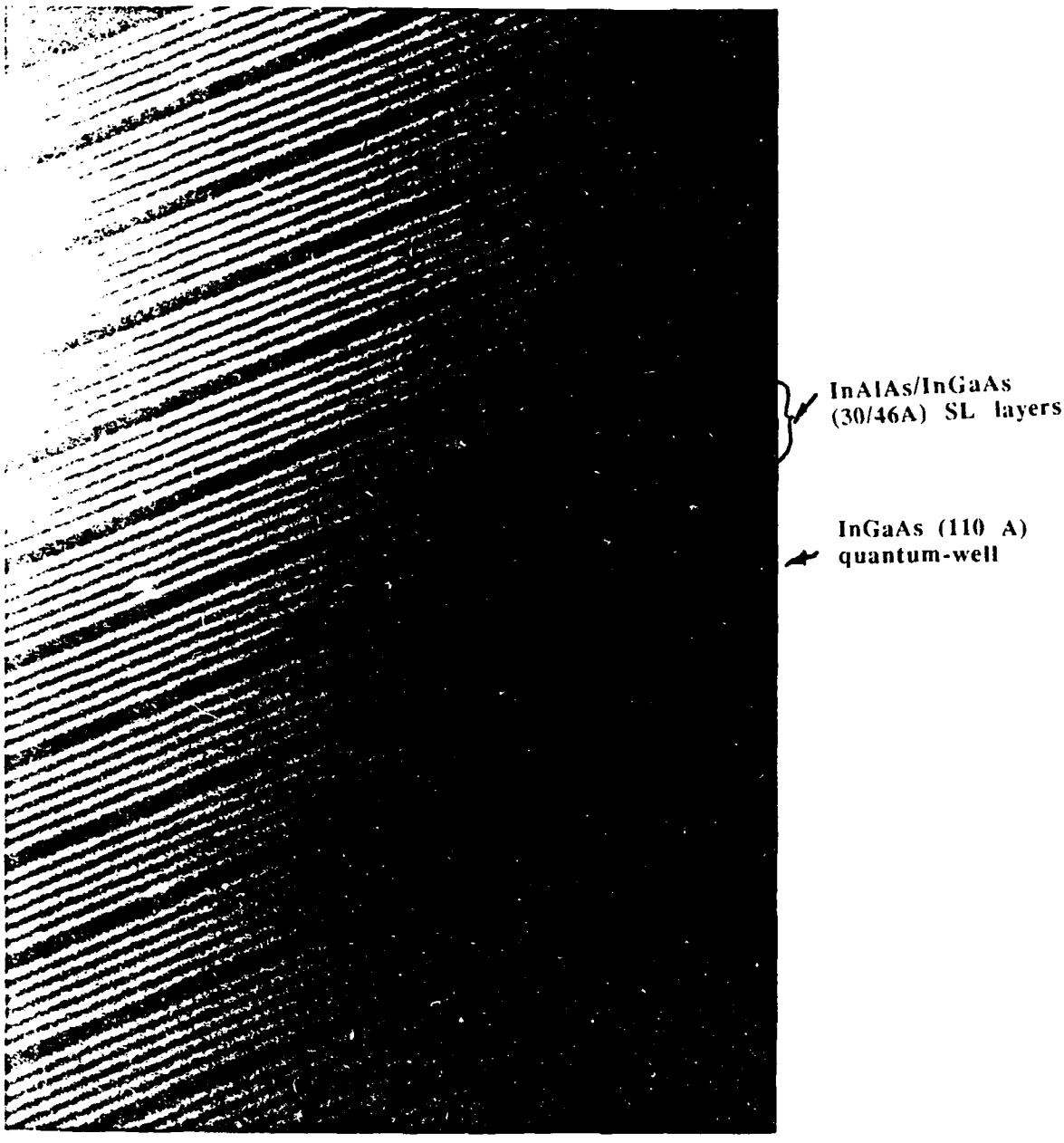

Fig.2.1 Cross sectional transmission electron microscopy (TEM) photograph for an InGaAs (110 A) multiquantum wells with short-period InAlAs (30 A)-InGaAs (46 A) superlattice barrier QWIP's.

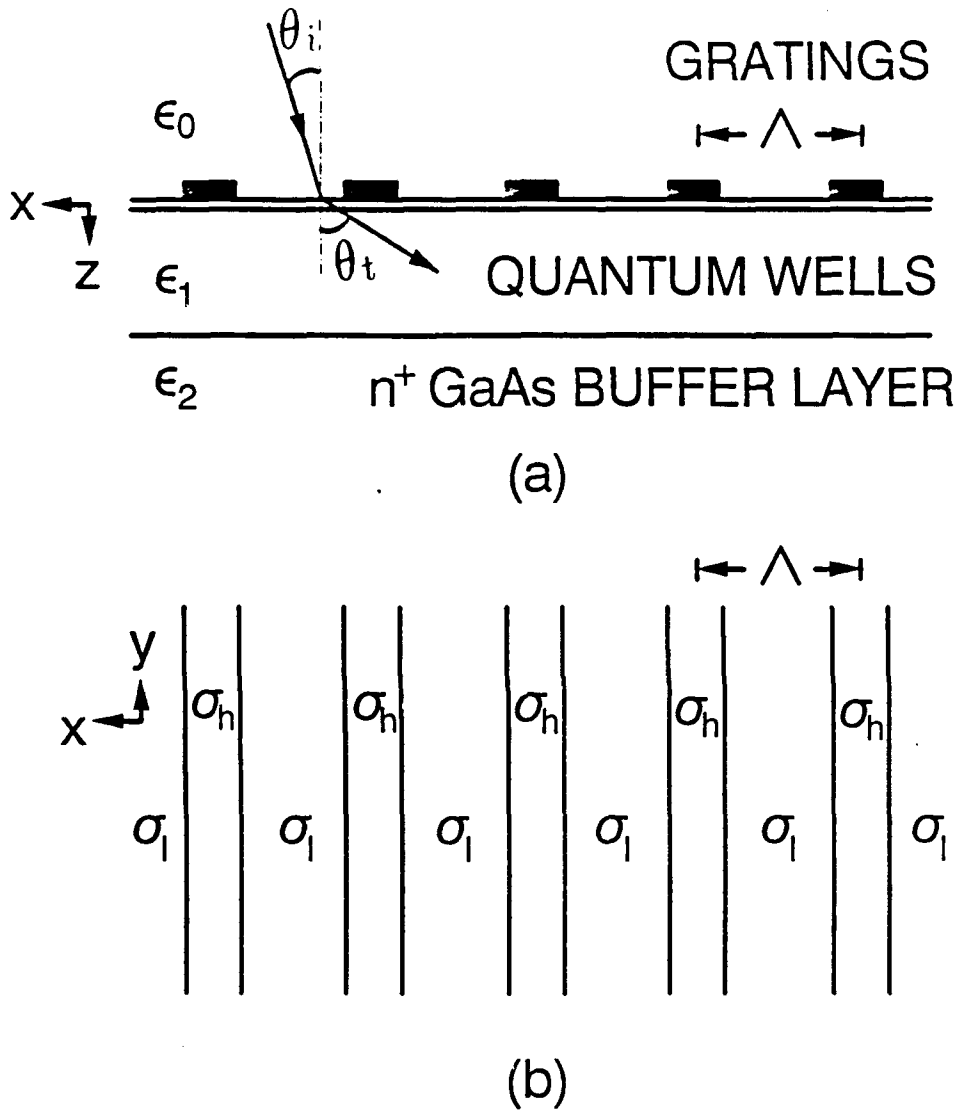

Figure 3.1 Configuration of a front incident strip metal grating coupler on a GaAs/AlGaAs multiple quantum well IR detector structure: (a) side view showing the grating periodicity Λ and diffraction angle θ_t, (b) top view of the grating modulation planes with alternated high conductivity (σ_h) and low conductivity (σ_l) regions.

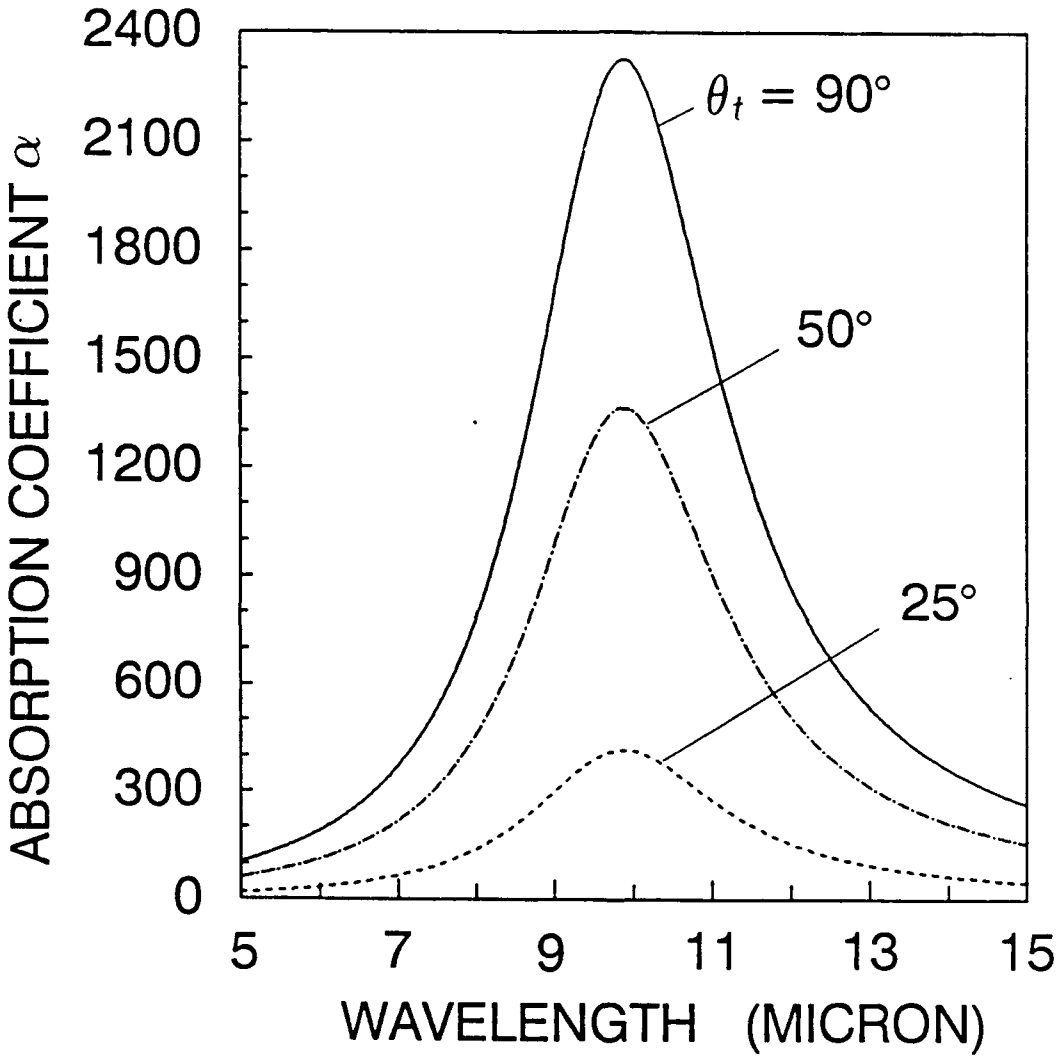

Figure 3.2 Calculated diffraction angle dependence of intersubband absorption $\alpha[\theta_t](cm^{-1})$ in the multiple quantum well layer.

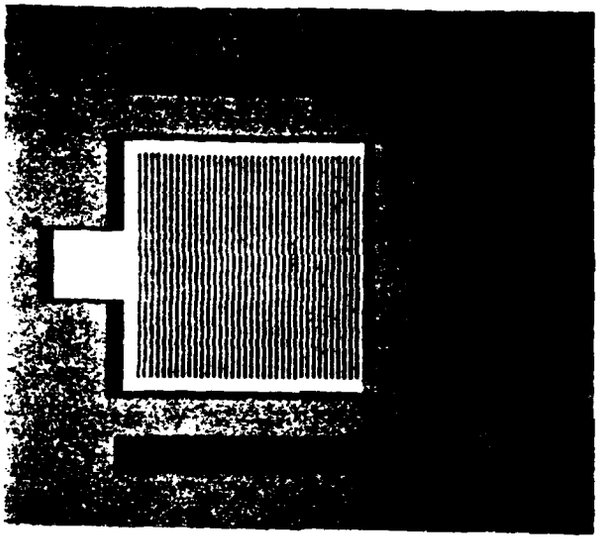

Figure 3.3 Top view of the fabricated AuGe/Ni/Au metal grating pattern with a 5 μm periodicity and a 200×200 μm^2 area for front side light coupling and ohmic contact.

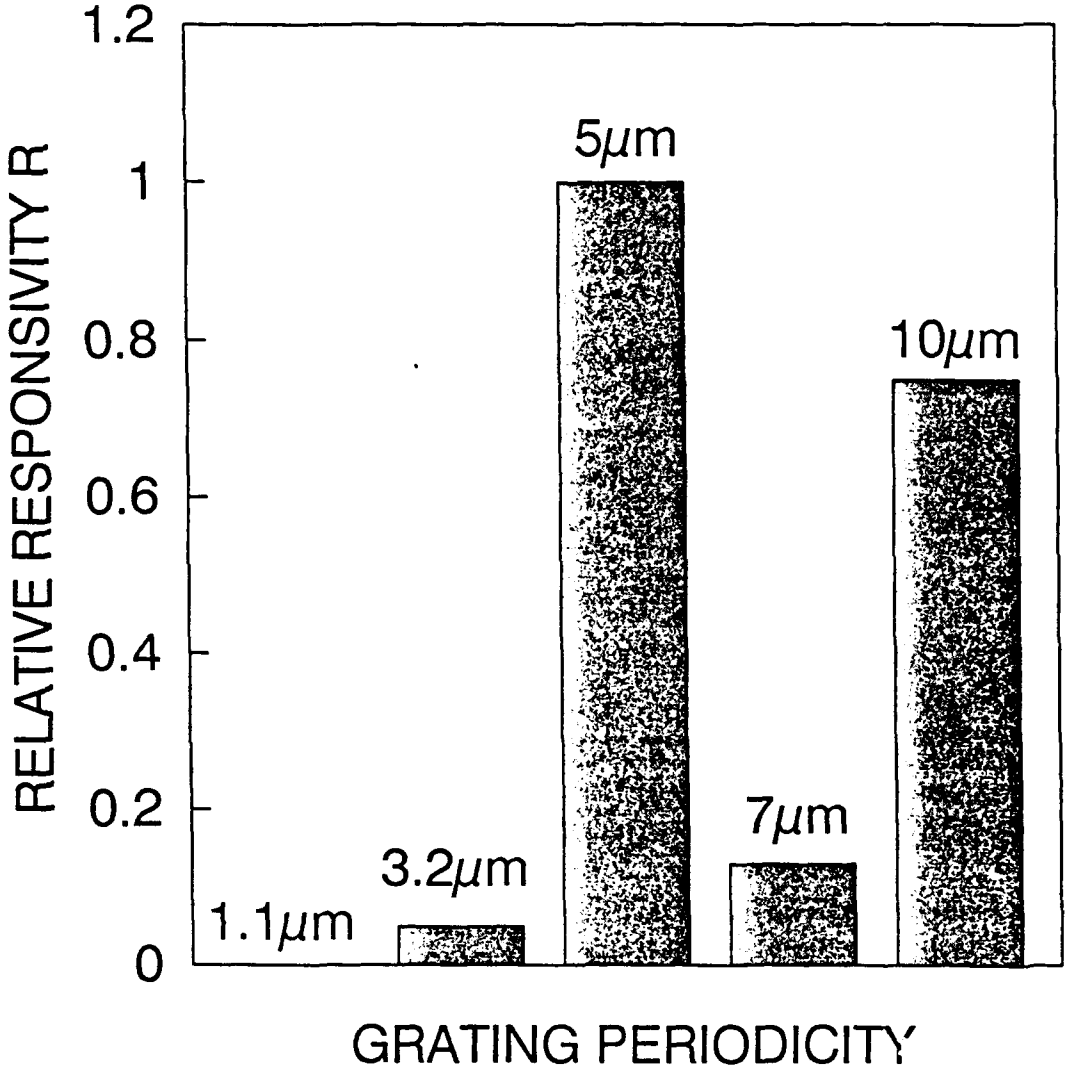

Figure 3.4 Measured relative responsivity versus grating periodicity for five different grating periodicities (1.1, 3.2, 5, 7, and 10 μm, respectively) at T = 77 K.

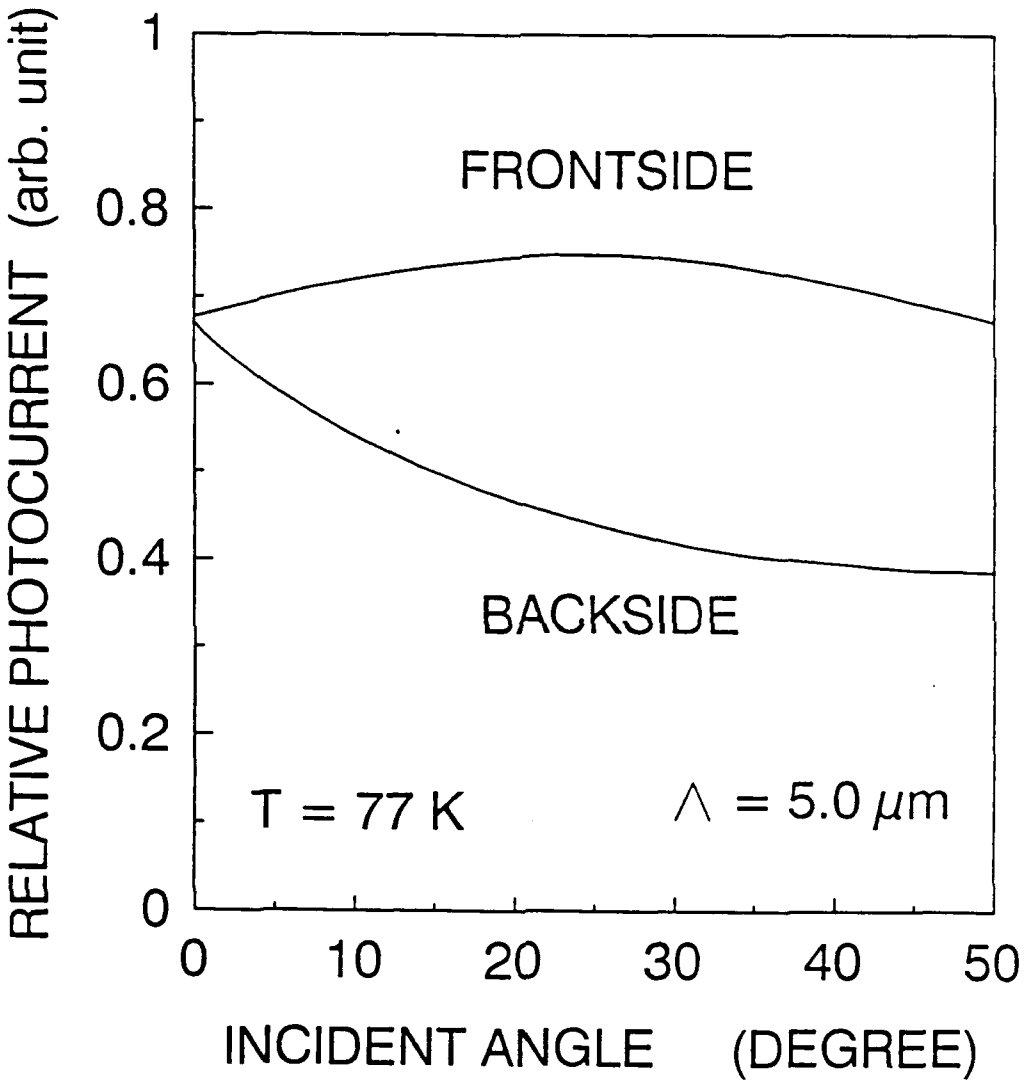

Figure 3.5 Relative photocurrent I_{ph} versus incident angle θ_i of IR radiations for the front side and backside illumination, using a 5 μm grating periodicity.

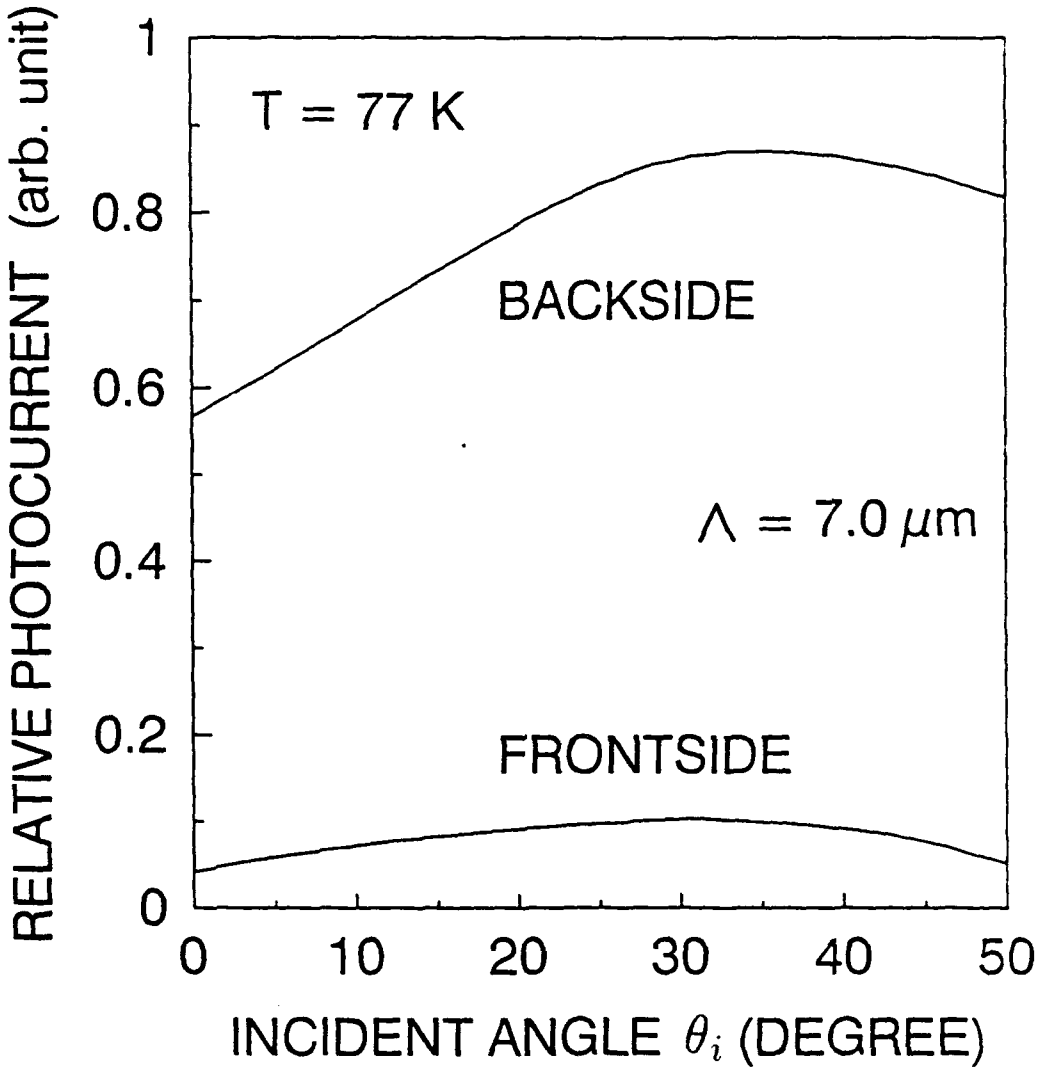

Figure 3.6 Relative photocurrent I_{ph} versus incident angle θ_i of IR radiation for the front side and back side illuminations, using a 7 μm grating periodicity.

3.2 Theoretical and Experimental Studies of Dark Current in the QWIPs

In a quantum well infrared photodetector (QWIP's), the dark current may be arised either from the thermionic emission or tunneling conduction, and must be kept very low in order to achieve excellent signal to noise ratio performance in such a detector. Therefore, it is extremely important to be able to predict the bias and temperature dependence of the dark current in a variety of long wavelength QWIPs.

In this section we report the theoretical calculations of the dark current as a function of temperature and bias voltage in two types of QWIPs. These include the conventional bound-to-continuum band (BTC) and the bound-to-miniband (BTM) transition GaAs/AlGaAs multiquantum well infrared detectors (QWIPs) [1-5]. A comparison of the calculated and the measured dark current values for both types of QWIPs is discussed in this section.

To calculate the dark current of a BTC QWIP composed of a 20-period multiquantum wells having a well width of 40 Å, a 480 Å barrier width, and a doping density in the well of $N_d = 1.4 \times 10^{18} cm^{-3}$ (referred to as sample A), we shall first determine the effective number of electrons n(V) which are excited out of the quantum well [1-2]:

$$n(V) = (\frac{m^*}{\pi \hbar^2 L_p}) \int_0^\infty f(E) T * T dE, \tag{1}$$

where L_p is the barrier width, f(E) is the Fermi distribution function, n(V) accounts for both the thermionic emission above the barrier and the thermionically assisted tunneling through the miniband. The dark current of a QWIP is given by

$$I_d(V) = n(V) e v(V) A \tag{2}$$

where e is the electronic charge, A is the device area, and $v(V)$ is the average electron velocity, which is field dependent and can be expressed as

$$v(V) = \frac{\mu \mathcal{E} + v_s (\mathcal{E}/\mathcal{E}_o)^4}{1 + (\mathcal{E}/\mathcal{E}_o)^4} \tag{3}$$

where $\mathcal{E}$ is the electric field, μ is the electron mobility, and $\mathcal{E}_o$ is the critical field. For GaAs, $\mu = 8,000\ cm^2/V.s.$, $v_s = 7.7 \times 10^6\ cm/s$, and $\mathcal{E}_o = 4 \times 10^3 V/cm$.

For the bound-to-miniband (BTM) transition GaAs/AlGaAs QWIP's (referred as sample B, as shown in Fig.3.7), the dark current is dominated by the thermionically assisted

tunneling conduction through the miniband inside the quantum well and superlattice barrier, whereas the thermionic emission above the superlattice barrier is negligible because of the high barrier ($\sim$ 390meV) for the BTM QWIP. To find the net tunneling current, we apply the formulism [6-8] of multibarrier tunneling to this QWIP's. The current density J may be computed as the average of the product of the transmission probability $T * T$ and the group velocity, $v(k) = \hbar^{-1} \nabla_k E$, which is given by

$$J = \frac{q}{4\pi^3\hbar} \int_0^\infty dk_l \int_0^\infty dk_t [f(E) - f(E')] T * T \frac{\partial E}{\partial k_l} \tag{4}$$

The transverse components of J are equal to zero by symmetry requirement [6]. Using separation of variables, the product $|T * T|$ is only a function of the longitudinal energy [8], and the longitudinal component of J becomes

$$J_l = \frac{4\pi q m^* kT}{h^3} \int_0^\infty T * T ln(\frac{1 + exp[(E_f - E_l)/kT]}{1 + exp[(E_f - E_l - qV_a)/kT]} dE_l \tag{5}$$

where V_a is the bias voltage across one period of superlattice barrier layer. Although variations of material properties with transmission coefficient T may cause a temperature dependence of $T * T$, it is far less sensitive to temperature comparing to the carrier energy distribution function, which is given by

$$g(E,V) = \frac{4\pi q m^* kT}{h^3} [ln(\frac{1 + exp[(E_f - E_l)/kT]}{1 + exp[(E_f - E_l - qV_a)/kT]})] \tag{6}$$

Since the tunneling process involves states in the partially filled, quasi-continuous conduction/valance bands, g(E,V) may vary more strongly with temperature. This variation is one of the main effects which governs the temperature behavior of the dark current in the QWIP's.

The bound-state energies of a one-dimensional finite potential well can be solved by using the time-independent Schroedinger equation. The solution in each region may be written as

$$\psi_i = \psi_i^+ e^{-i(\Delta_i + ik_i x)} + \psi_i^- e^{i(\Delta_i - ik_i x)} \tag{7}$$

where

$$\begin{aligned} \Delta_1 &= \Delta_2 = 0, \\ \Delta_i &= k_i(d_2 + d_3 + \cdots + d_{i-1}); \\ i = 3,4,\cdots \qquad k_i &= \frac{2m^*}{h^2}(E - V_i)]^{1/2} \end{aligned} \tag{8}$$

where ψ_i^+ and ψ_i^- represents the amplitude of the wave propagating along the $+x$ and $-x$ directions, respectively. Continuity of the wave functions and its derivative at each interface gives [9]

$$\begin{pmatrix} \psi_1^+ \\ \psi_1^- \end{pmatrix} = S_1 \begin{pmatrix} \psi_2^+ \\ \psi_2^- \end{pmatrix} = S_1 S_2 \begin{pmatrix} \psi_3^+ \\ \psi_3^- \end{pmatrix}$$

$$= \cdots = S_1 S_2 \cdots S_{N-1} \begin{pmatrix} \psi_N^+ \\ \psi_N^- \end{pmatrix} \tag{9}$$

where

$$S_i = \frac{1}{t_i} \begin{pmatrix} e^{-\delta_i} & r_i e^{-\delta_i} \\ r_i e^{-\delta_i} & e^{i\delta_i} \end{pmatrix}, \qquad \delta_i = k_i d_i$$

$$r_i = \frac{k_i - k_{i+1}}{k_i + k_{i+1}}$$

$$t_i = \frac{2k_i}{k_i + k_{i+1}} \tag{10}$$

If we assume region N as the ohmic contact and $\psi_N^- = 0$, then we can calculate the wave function in any regions of the device in terms of ψ_N^+. Thus, the transmission probability can be written as

$$T * T = \left| \frac{\psi_m^+}{\psi_1^+} \right|^2 \tag{11}$$

where ψ_m^+ is the wave function of an electron tunneling into the mth quantum well of the QWIP.

Figure 3.8 and Fig.3.9 show the transmission probability $T * T$ versus electron energy under different bias conditions for sample A and sample B, respectively. In the calculations of dark current we have assumed that the field is uniformly distributed over the low-conducting superlattice (SL) barrier layer regions. The voltage (V_a) cross each period of superlattice is assumed equal to the bias voltage V divided by the number of SL period. It is obvious that for sample A at low bias (V $\leq$1 V) most of the carriers are escaped from the quantum wells into the continuum band over the top of the barrier, whereas for sample B the dark current is due to carriers tunnelling through the miniband inside the quantum wells and the superlattice barrier layer.

Figure 3.10 shows the measured dark current as a function of temperature and bias voltage for sample B with an area $A = 4 \times 10^{-4} cm^2$ and doping concentration $N_d = 2.0^{18} cm^{-3}$. Note that a negative differential conductance was observed for temperature below 55 K, implying that resonance tunneling current is significant at very low temperatures.

The calculated and measured dark current for sample A and sample B are shown in Fig.3.11 and Fig.3.12, respectively. In the calculation, we assumed that the electron mean free path was long enough for carriers to traverse several periods without losing coherence due to scattering and neglected its field dependence. At low bias the dark current I_d is expected to increase exponentially with temperature [10] and can be expressed by

$$I_d \propto exp(\frac{-\Delta E}{kT}) \tag{12}$$

where ΔE is the thermal activation energy. In order to confirm this dependence, the I_d vs. V curves shown Fig.3.11 and Fig.3.12 were replotted as a function of temperature, and the results were shown in Fig.3.13 and Fig.3.14 for $V = 0.1$ V , respectively. From the slope of this plot we found $\Delta E = 105.4$ meV for sample A and $\Delta E = 99.8$ meV for sample B. As expected, both ΔE are in good agreement with that obtained from Fig.3.8 and Fig.3.9.

Although results of our calculations presented in this section showed reasonable agreement with that of the experimental data, further study such as high field phenomenon, carrier transport mechanism is needed in order to precisely predict the dark current in the QWIPs, and hence allow us to optimize the device parameters. Our next step is to accurately calculate the parameters of a step-bound-to-miniband (SBTM) QWIP by modifying the parameters for a real device, and design new QWIP's structures by optimizing the predictable parameters.

References

1. B. F. Levine, C. G .Bethea, G.Hasnain, V.O. Shen, E. Pelve, and R.R. Abbott Appl. Phys. Lett. 56(9), 26 (1990).

2. A. Zussman, B. F. Levine, J. M. Kuo and de Jong, J. appl. phys. 70, p.5106 (1991).

3. L. S. Yu and S. S. Li, Appl. Phys. Lett. 59(11),1332 (1991).

4. L. S. Yu and S. S. Li. Appl. Phys. Lett. 59(21),2712 (1991).

5. L. S. Yu, S. S. Li, and Y. C. Kao, Proc. of the Government Microcircuit Applications Conference, Vol. XVI. Nov. 6-8, Las Vegas, Nevada, pp. 179 (1990).

6. R. Tsu and L Esaki. Appl. Phys. Lett. 22(11),562 (1973).

7. M. O. Vassel, J. Lee, and H.F. Lockwood, J. Appl. Phys 54(9),5206 (1983).

8. G. D. Shen, D. X. Xu, M. Willander, and G. V. Hansson. Appl. Phy. Lett. 58(7),738 (1991).

9. C. B. Duke, Academic. New York, p.32 (1969).

10. A. K. Ghatak, K. Thyagarajan, and M. R. Shenoy, IEEE J. of Quantum Elctronics. Vol. 24, no. 8, Aug (1988).

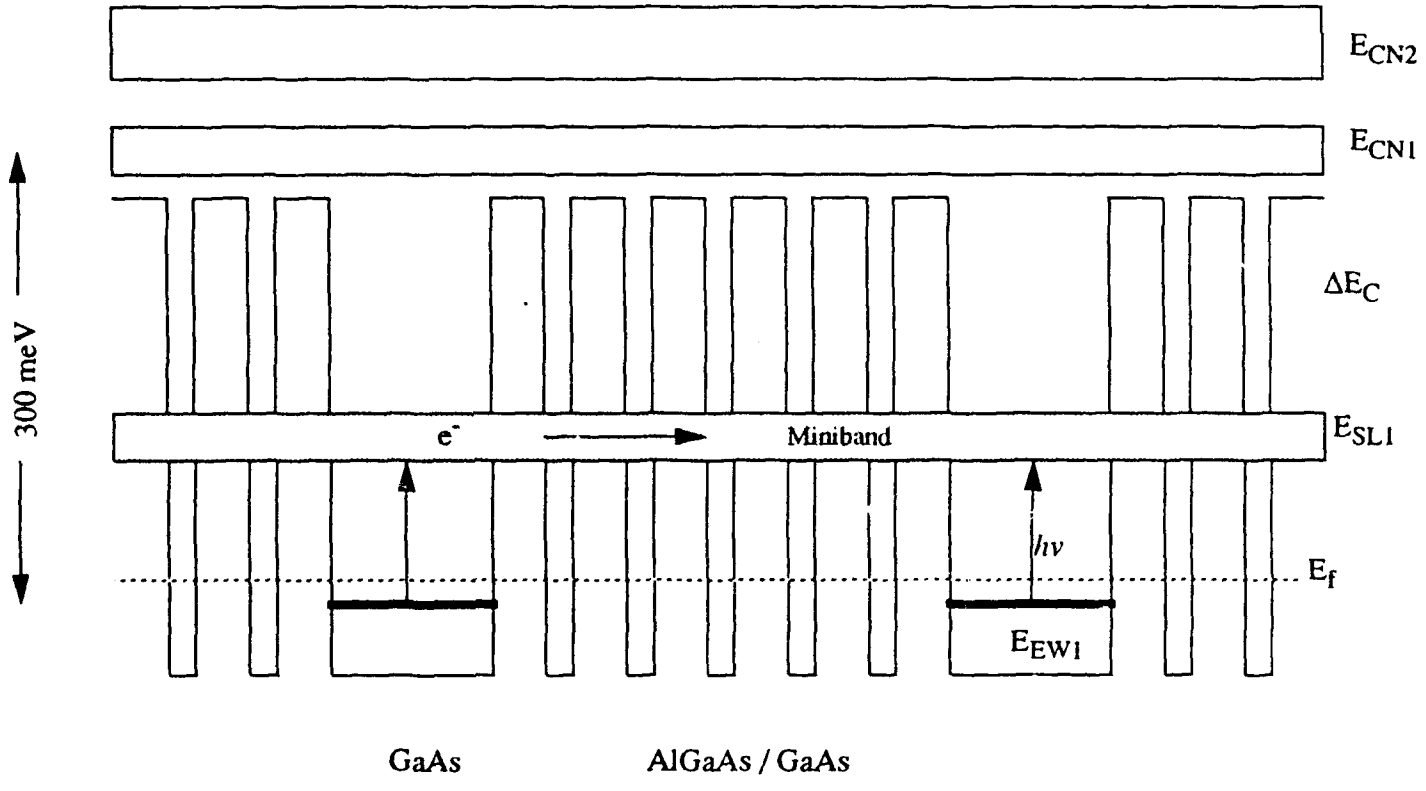

Figure 3.7 Energy band diagram for a bound-to-miniband (BTM) transition GaAs/AlGaAs QWIP's.

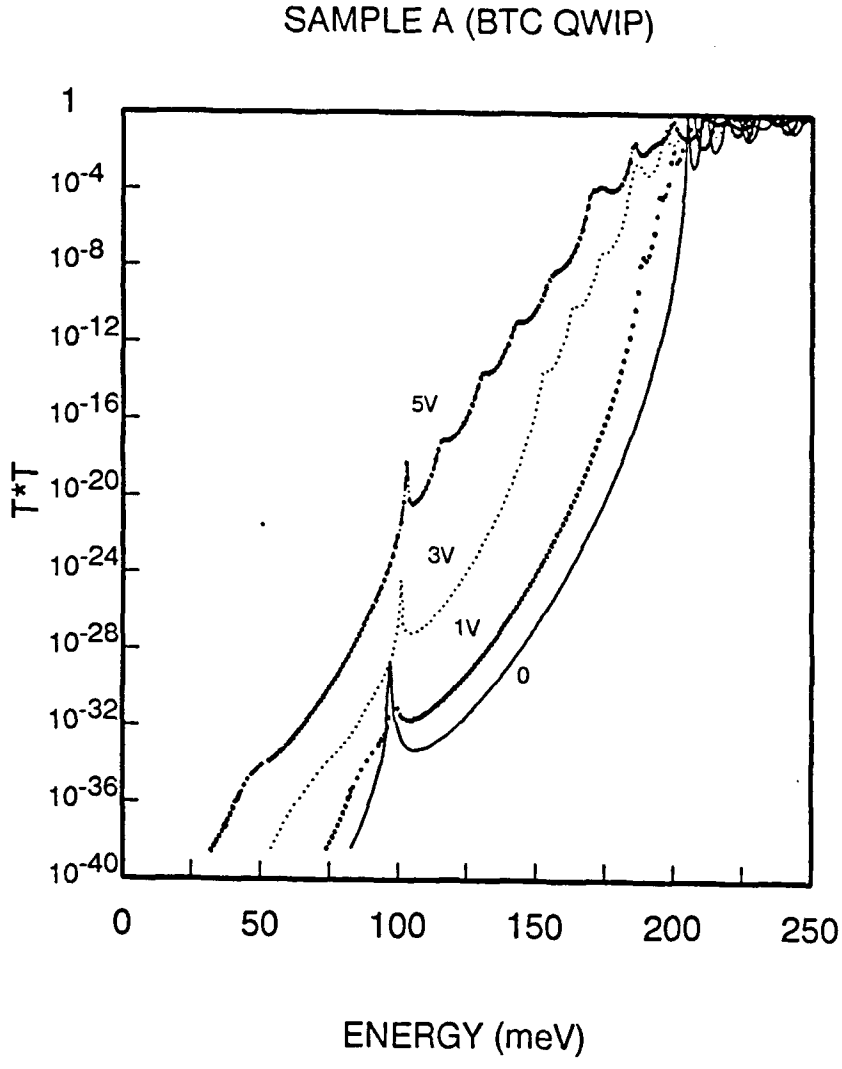

Figure 3.8 The calculated transmission probability $T * T$ versus electron energy under different bias conditions for the bound-to-continuum band (BTC) GaAs/AlGaAs QWIP's (sample A).

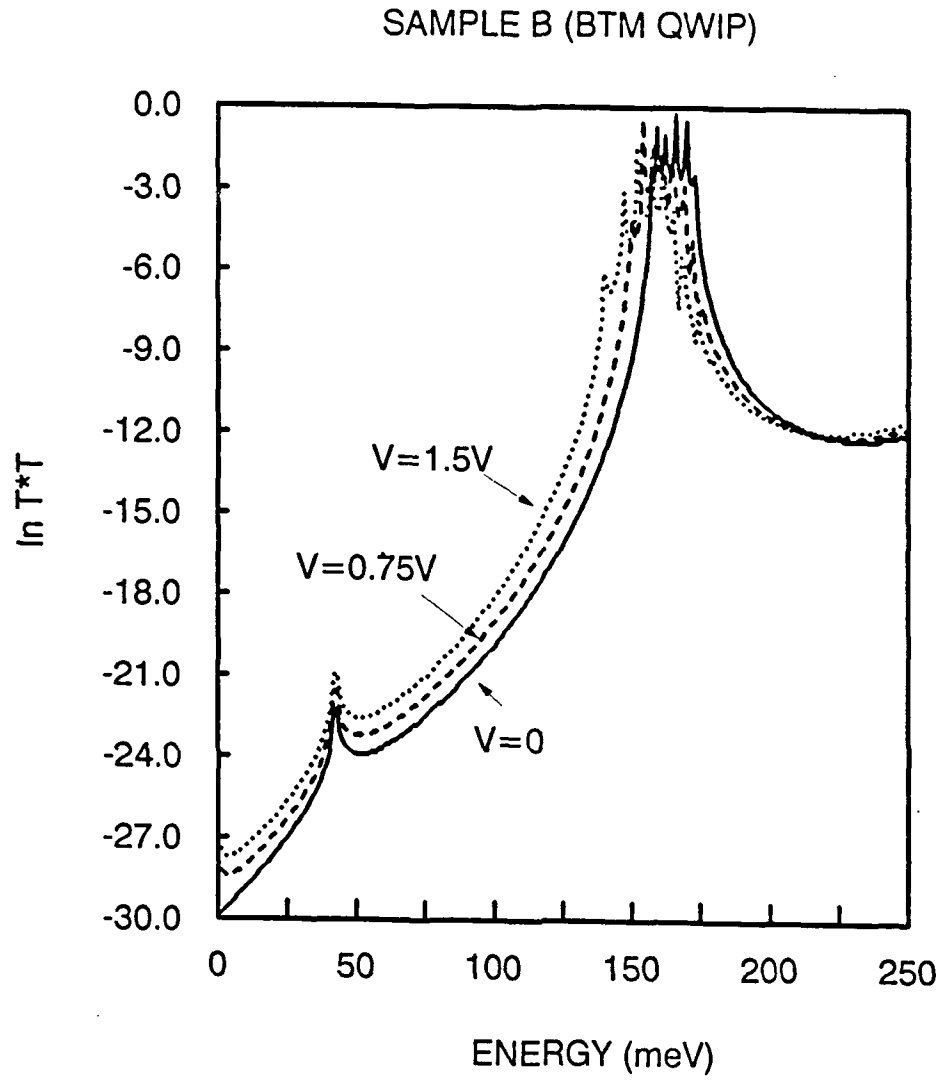

Figure 3.9 The calculated transmission probability $T * T$ versus electron energy under different bias conditions for the bound-to-miniband band (BTM) GaAs/AlGaAs QWIP's (sample B).

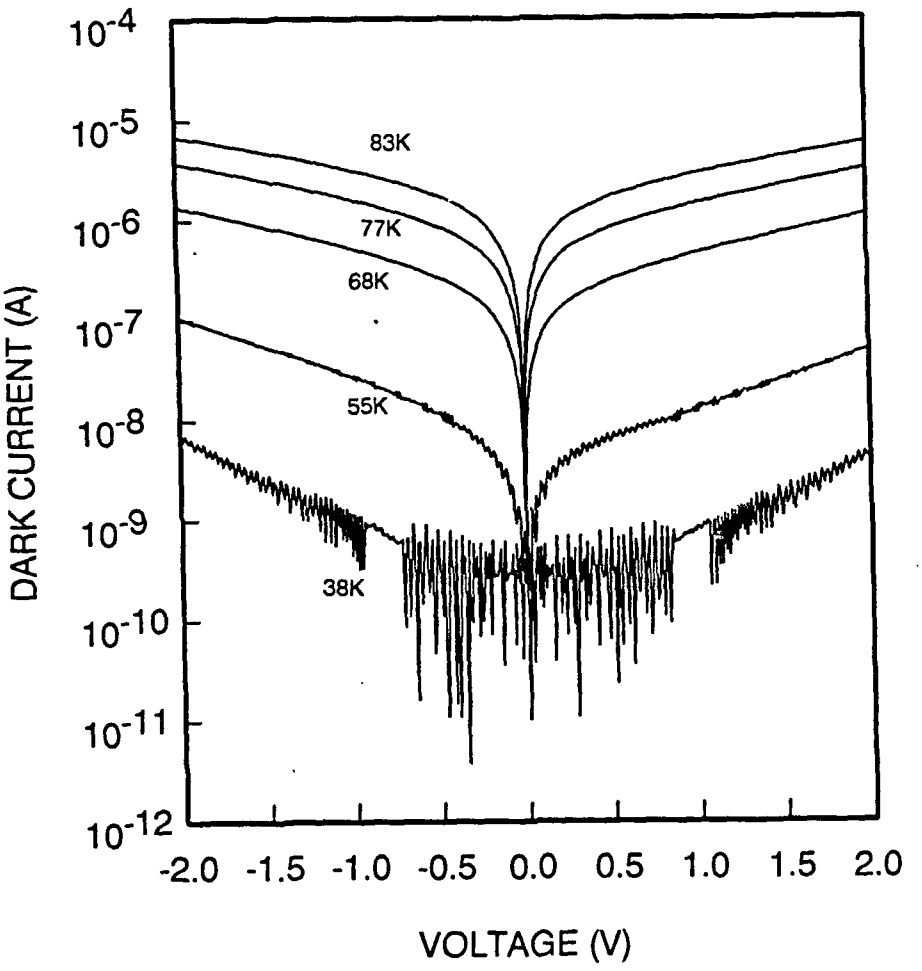

Figure 3.10 The measured dark current as a function of bias voltage and temperature for the bound-to-miniband band (BTM) GaAs/AlGaAs QWIP's (sample B).

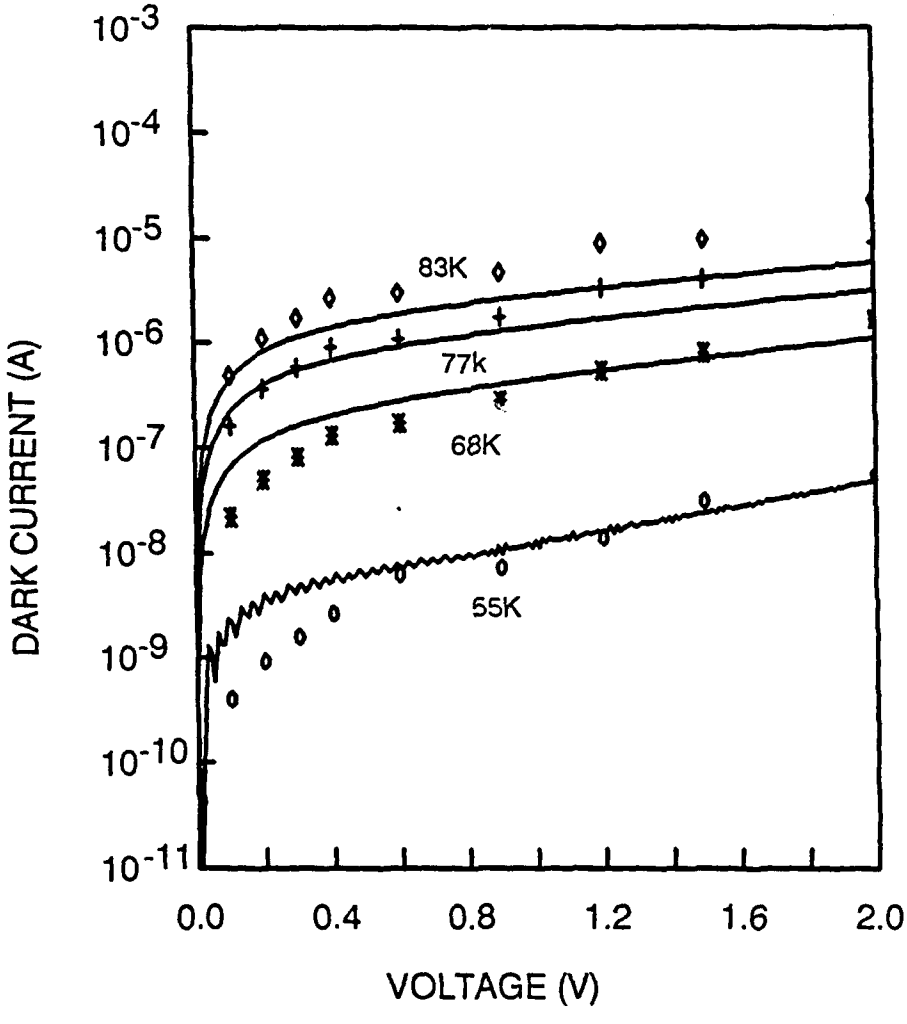

Figure 3.11 The measured and calculated dark current as a function of bias voltage and temperature for the bound-to-miniband band (BTM) GaAs/AlGaAs QWIP's (sample B).

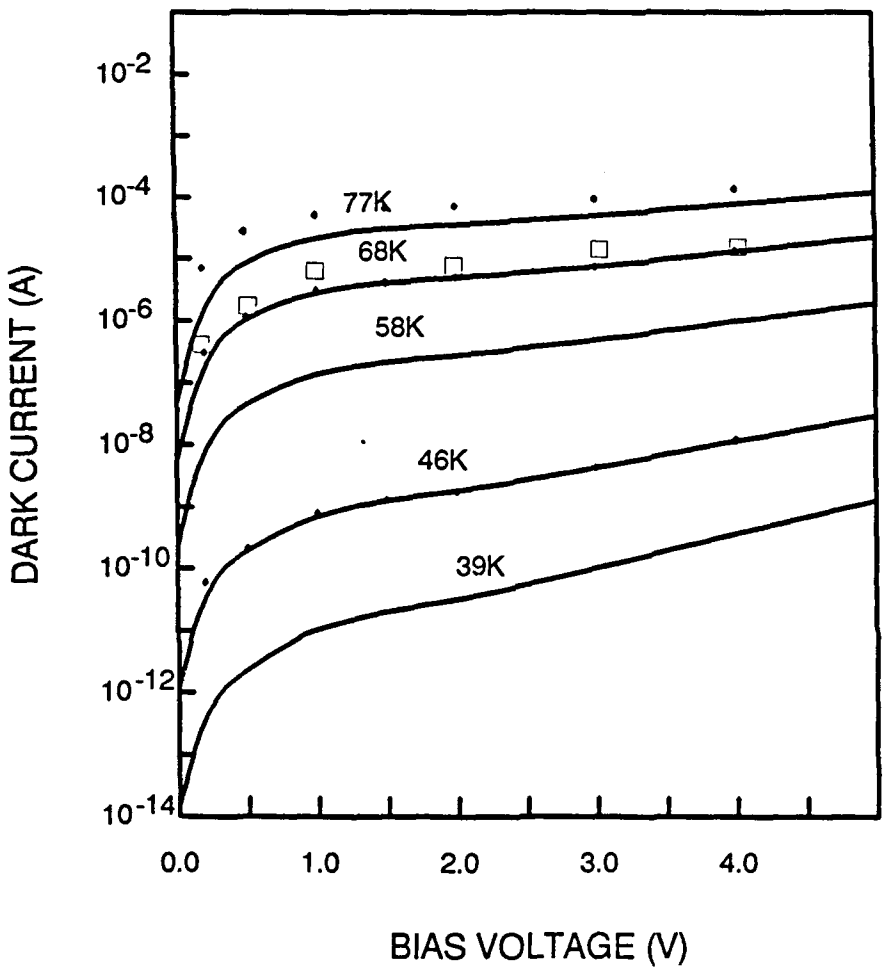

Figure 3.12 The measured and calculated dark current as a function of bias voltage and temperature for the bound-to-continuum band (BTC) GaAs/AlGaAs QWIP's (sample A).